Neutron skin thickness and equation of state in asymmetric nuclear matter

Satoshi Yoshida[1,*] and Hiroyuki Sagawa[2]
[1]*Science Research Center, Hosei University, 2-17-1 Fujimi, Chiyoda, Tokyo 102-8160, Japan*
[2]*Center for Mathematical Sciences, the University of Aizu, Aizu-Wakamatsu, Fukushima 965-8580, Japan*
(Received 23 May 2003; published 27 February 2004)

The neutron skin thickness of stable and unstable nuclei is studied in Skyrme Hartree-Fock (SHF) and relativistic mean field (RMF) models to investigate the relation between the pressure and the equation of state in neutron matter. We found a clear linear correlation between the neutron skin thickness in heavy nuclei ^{132}Sn and ^{208}Pb and the pressure of neutron matter in both SHF and RMF models, while the correlation is weak in the unstable nuclei ^{32}Mg and ^{44}Ar. Relations between the neutron skin thickness and other nuclear matter properties such as the symmetry energy coefficients and the nuclear incompressibility are discussed.

DOI: 10.1103/PhysRevC.69.024318 PACS number(s): 21.10.Pc, 21.60.−n, 21.90.+f

I. INTRODUCTION

The proton and neutron density distributions are some of the most fundamental observables of nuclei. Charge radii of nuclei are derived from charge density distributions which can be determined to a high accuracy in experiments using electromagnetic probes, for example, electron scattering experiments [1]. The empirical information of proton radii is then obtained from these charge radii. In contrast, it is much more difficult to accurately determine the neutron density distributions of nuclei by any experimental probe [2]. Several attempts have been made to determine the neutron density distributions by using proton scattering and interaction cross sections in heavy ion collisions at relativistic energies [3]. So far, the accuracy of neutron radii determinations is poor compared to that of proton radii. However, a promising experiment to determine the neutron radius has been proposed, namely, to measure the parity violation effect in polarized electron scattering [4].

Nuclei for which the neutron number N is larger than the proton number Z are expected to have a neutron skin. Its thickness depends on the balance between various aspects of the nuclear force. The isospin asymmetry properties of the nuclear force favor equal proton and neutron densities at each spatial location, that is, $\rho_{\rm p}(x,y,z)=\rho_{\rm n}(x,y,z)$. However, when $N\neq Z$ this condition cannot be fulfilled everywhere. The actual proton and neutron density distributions are determined by the balance between the isospin asymmetry and the Coulomb force. Also for the case $N=Z$ these forces cause slight deviations from $\rho_{\rm p}(x,y,z)=\rho_{\rm n}(x,y,z)$. In mean-field calculations, the skin thickness is related to the disparity in the Fermi energies between protons and neutrons [5,6]. This disparity is the main cause of the difference between the neutron and the proton radii in unstable nuclei. On the other hand, in stable nuclei where the neutron and the proton Fermi energies are similar, the neutron skin thickness is created by the pressure of the nuclear medium and is much smaller than in unstable nuclei. Accordingly the size of the neutron skin thickness will give an important constraint on the pressure of the equation of state (EOS), which is an essential ingredient for the calculation of the properties of neutron stars [7]. It was pointed out that the neutron skin thickness of ^{208}Pb is strongly correlated with the pressure (the first derivative) of EOS at neutron density $\rho_{\rm n}=0.1$ fm^{-3} in the Skyrme Hartree-Fock (SHF) model [8] and in the relativistic models [9]. The neutron skin thickness in ^{208}Pb was discussed also in the context of effective field theory in Ref. [10]. A similar pressure-EOS correlation was found also in ^{138}Ba and ^{132}Sn. In this paper, we study the neutron skin thickness of stable nuclei, and of several unstable nuclei by use of SHF and relativistic mean field (RMF) models. The aim of this paper is twofold. First, we extend the study of the correlations between the neutron skin thickness and the pressure of EOS to some light unstable nuclei, which can be accessed in radioactive ion beam experiments. Second, we study the relations between the neutron skin thickness and other nuclear matter properties such as the volume and surface symmetry energy coefficients and the nuclear incompressibility. The mean field models are summarized in Sec. II. Section III is devoted to studies of the relation between the neutron skin thickness and the pressure of the EOS. Relations between the neutron skin thickness and the volume and surface symmetry energy coefficients are discussed in Sec. IV. A summary is given in Sec. V. Detailed discussions of symmetry energy coefficients are given in the Appendix.

II. MODEL

The SHF model for finite nuclei is implemented with a density-dependent pairing force for BCS calculations. The Skyrme force $V_{\rm Sky}$ is an effective zero-range force with density-dependent and momentum-dependent terms [11],

$$\begin{aligned}V_{\rm Sky}(\vec{r}_1,\vec{r}_2) &= t_0(1+x_0P_\sigma)\,\delta(\vec{r}_1-\vec{r}_2)+\tfrac{1}{2}t_1(1+x_1P_\sigma)\{\vec{k}'^2\delta\\ &\quad\times(\vec{r}_1-\vec{r}_2)+\delta(\vec{r}_1-\vec{r}_2)\vec{k}^2\}+t_2(1+x_2P_\sigma)\vec{k}'\cdot\delta\\ &\quad\times(\vec{r}_1-\vec{r}_2)\vec{k}+\tfrac{1}{6}t_3(1+x_3P_\sigma)\rho^{\alpha}(\vec{r})\,\delta(\vec{r}_1-\vec{r}_2)\\ &\quad+iW(\vec{\sigma}_1+\vec{\sigma}_2)\cdot\vec{k}'\times\delta(\vec{r}_1-\vec{r}_2)\vec{k},\end{aligned} \tag{1}$$

where $\vec{k}=(\vec{\nabla}_1-\vec{\nabla}_2)/(2i)$ acting on the right and $\vec{k}'=-(\overleftarrow{\nabla}_1$

*FAX: 81-3-3264-9429; Email address: s_yoshi@i.hosei.ac.jp

$-\overleftarrow{\nabla}_2)/(2i)$ acting on the left are the relative momentum operators, P_σ is the spin exchange operator, $\vec{\sigma}$ is the Pauli spin matrix, and $\vec{r}=\frac{1}{2}(\vec{r}_1+\vec{r}_2)$. The interaction (1) simulates the G matrix for nuclear Hartree-Fock calculations. The Hamiltonian density for Skyrme Hartree-Fock calculation is

$$\begin{aligned}\mathcal{H}(\rho_n,\rho_p) &= \frac{\hbar^2}{2m}(\tau_n+\tau_p)+\frac{1}{4}t_0(1-x_0)(\rho_n^2+\rho_p^2)+t_0\left(1+\frac{1}{2}x_0\right)\rho_n\,\rho_p+\frac{1}{12}t_3\left(1+\frac{1}{2}x_3\right)\rho^{\alpha+2}-\frac{1}{12}t_3\left(\frac{1}{2}+x_3\right)\rho^{\alpha}(\rho_n^2+\rho_p^2)\\ &\quad+\frac{1}{8}[t_1(1-x_1)+3\,t_2(1+x_2)](\rho_n\tau_n+\rho_p\tau_p)+\frac{1}{4}\left[t_1\left(1+\frac{1}{2}x_1\right)+t_2\left(1+\frac{1}{2}x_2\right)\right](\rho_n\tau_p+\rho_p\tau_n)-\frac{3}{32}[t_1(1-x_1)\\ &\quad-t_2(1+x_2)](\rho_n\nabla^2\rho_n+\rho_p\nabla^2\rho_p)-\frac{1}{16}\left[3\,t_1\left(1+\frac{1}{2}x_1\right)-t_2\left(1+\frac{1}{2}x_2\right)\right](\rho_n\nabla^2\rho_p+\rho_p\nabla^2\rho_n)-\frac{1}{2}W(\rho\vec{\nabla}\cdot\vec{J}+\rho_n\vec{\nabla}\cdot\vec{J}_n\\ &\quad+\rho_p\vec{\nabla}\cdot\vec{J}_p)+\mathcal{H}_{\text{Coul}}-\frac{1}{16}(t_1x_1+t_2x_2)\vec{J}^2+\frac{1}{16}(t_1-t_2)(\vec{J}_n^2+\vec{J}_p^2),\end{aligned}\tag{2}$$

where $\rho_n(\rho_p)$ is the density of neutrons (protons) and $\rho=\rho_n+\rho_p$, while $\tau_n(\tau_p)$ and $\vec{J}_n(\vec{J}_p)$ are the kinetic energy and the spin-orbit densities of neutrons (protons), respectively. The neutron skin thickness of stable and unstable heavy nuclei is studied within the SHF model using 18 different parameter sets (SI–SIV, Skya, Skyb, SkM, SkM*, SGI, SGII, SkI3, SkI4, MSkA, SLy4, SLy10, SkX) taken from Refs. [8,12–20]. The modified form of spin-orbit interaction was adopted in the case of SkI3, SkI4, SLy10, MSkA, and SkX. The spin-orbit density terms in Eq. (2) are omitted in the HF calculations except for SLy10.

A density-dependent zero-range force is adopted as a pairing interaction for SHF+BCS calculations,

$$V_{\text{pair}}=\frac{V_0}{2}(1-P_\sigma)\left(1-\frac{\rho(\vec{r}_1)}{\rho_c}\right)\delta(\vec{r}_1-\vec{r}_2),\tag{3}$$

where the critical density ρ_c is taken to be 0.16 fm^{-3} and the strength V_0 is equal to -880 MeV fm^3 for heavy nuclei and -400 MeV fm^3 for light nuclei. The strength V_0 is fixed to be either -880 MeV fm^3 or -400 MeV fm^3 in all Skyrme parameter sets, although this value might be determined depending on the level density around the Fermi energy, i.e., the effective mass of each Skyrme interaction [20]. We investigated $V_0=-1000$ MeV fm^3 for SLy4 in ^{133}Ba. The averaged gap energy then increases by 21%, whereas the change in δ_{np} is less than 0.6%. Since the main aim of the present study is the value δ_{np}, we choose to use a fixed V_0 value for all Skyrme interactions depending on the mass of nucleus. In order to avoid divergences of the pairing energy, an energy cutoff parameter is introduced in the valence single-particle space above the Fermi level to limit the active pairing space to one major shell. We use the cutoff prescription of the model space in Ref. [21].

Next, we summarize the formulation of the RMF model with nonlinear meson couplings. The following relativistic Lagrangian (density) $\mathcal{L}$ is adopted for the interacting many-body system consisting of nucleons, scalar σ, and vector ω, and charged $\vec{\rho}$ mesons, and photons [22–27],

$$\begin{aligned}\mathcal{L} &= \bar{\psi}\left(i\gamma^\mu\partial_\mu-M-g_\sigma\sigma-g_\omega\gamma^\mu\omega_\mu-g_\rho\gamma^\mu\vec{\tau}\vec{b}_\mu\right.\\ &\quad\left.-e\gamma^\mu\frac{1-\tau_3}{2}A_\mu\right)\psi+\frac{1}{2}(\partial_\mu\partial^\mu\sigma-m_\sigma^2\sigma^2)-U(\sigma)\\ &\quad+\frac{1}{2}m_\omega^2\omega_\mu\omega^\mu-\frac{1}{4}F_{\mu\nu}F^{\mu\nu}+\frac{1}{2}m_\rho^2\vec{b}_\mu\vec{b}^\mu-\frac{1}{4}\vec{G}_{\mu\nu}\vec{G}^{\mu\nu}\\ &\quad-\frac{1}{4}H_{\mu\nu}H^{\mu\nu},\end{aligned}\tag{4}$$

where $F_{\mu\nu}\equiv\partial_\mu\omega_\nu-\partial_\nu\omega_\mu$, $\vec{G}_{\mu\nu}\equiv\partial_\mu\vec{b}_\nu-\partial_\nu\vec{b}_\mu$, $H_{\mu\nu}\equiv\partial_\mu A_\nu-\partial_\nu A_\mu$, and $\sigma,\omega_\mu,\vec{b}_\mu$, and A_μ are the σ, ω, ρ mesons, and the electromagnetic field, respectively. The quantities g_σ, g_ω, and g_ρ are the coupling constants between nucleons and σ, ω, and ρ mesons, respectively, while $e^2/4\pi=1/137$ is the fine structure constant. The quantities m_σ,m_ω,m_ρ, and M are the masses of σ,ω, ρ mesons, and nucleons, respectively. The quantity $U(\sigma)$ is the nonlinear potential of σ mesons [28],

$$U(\sigma)=\tfrac{1}{3}g_1\sigma^3+\tfrac{1}{4}g_2\sigma^4,\tag{5}$$

where g_1 and g_2 are parameters of the potential. The Dirac equation for nucleons and the Klein-Gordon equations for mesons are derived by the classical variational principle with time-reversal symmetry and charge conservation,

$$\begin{aligned}&\left[-i\vec{\alpha}\cdot\vec{\nabla}+\beta M^*+g_\omega\omega(\vec{r})+g_\rho\tau_3 b(\vec{r})+e\frac{1-\tau_3}{2}A(\vec{r})\right]\psi_i(\vec{r})\\ &\quad=\varepsilon_i\psi_i(\vec{r}),\end{aligned}\tag{6}$$

$$(-\nabla^2+m_\sigma^2)\sigma(\vec{r})=-g_\sigma\rho_s(\vec{r})-g_1\sigma^2(\vec{r})-g_2\sigma^3(\vec{r}),$$

$$(-\nabla^2 + m_\omega^2)\omega(\vec{r}) = g_\omega \rho_B(\vec{r}),$$

$$(-\nabla^2 + m_\rho^2)b(\vec{r}) = g_\rho \rho_3(\vec{r}),$$

$$-\nabla^2 A(\vec{r}) = e\rho_{\rm p}(\vec{r}), \qquad (7)$$

where $\vec{\alpha}$ and β are defined by

$$\vec{\alpha} = \begin{pmatrix} 0 & \vec{\sigma} \\ \vec{\sigma} & 0 \end{pmatrix} \quad \text{and} \quad \beta = \begin{pmatrix} I & 0 \\ 0 & -I \end{pmatrix},$$

where $\vec{\sigma}$ is the Pauli matrix and I is the 2×2 unit matrix, respectively. The baryon and the scalar densities are denoted by ρ_B and ρ_s, respectively, while $\rho_3 = \rho_{\rm n} - \rho_{\rm p}$ is the isovector density. The effective mass M^* is defined by $M^* = M + g_\sigma \sigma$. The RMF model is applied only to closed-shell nuclei without a pairing interaction. Five different parameter sets (NL1–NL3, NLSH, and NLC) taken from Refs. [22,29–31] are studied.

III. EQUATION OF STATE AND PRESSURE FOR NEUTRON MATTER

The pressure P of neutron matter is defined as the first derivative of Hamiltonian density with respect to the neutron density,

$$P = \rho_{\rm n}^2 \frac{d}{d\rho_{\rm n}}\left(\frac{\mathcal{H}}{\rho_{\rm n}}\right), \qquad (8)$$

where $\mathcal{H}$ is the Hamiltonian density of neutron matter $\mathcal{H}(\rho_{\rm n}, \rho_{\rm p}=0)$. The Thomas-Fermi approximation of the Hamiltonian density of the SHF model for infinite nuclear matter is used and the derivative terms and the Coulomb term are neglected. In the RMF calculations, the static Hamiltonian density of nuclear matter can be obtained by using Eqs. (6) and (7) [25],

$$\mathcal{H}_{\rm nm} = \frac{2}{(2\pi)^3}\left[\int_0^{k_{F_{\rm p}}} + \int_0^{k_{F_{\rm n}}}\right](k^2 + M^{*2})^{1/2}\, d^3k + g_\omega \omega \rho_B - \frac{1}{2}m_\omega^2\omega^2 + U(\sigma) + \frac{1}{2}m_\sigma^2\sigma^2 + g_\rho b \rho_3 - \frac{1}{2}m_\rho^2 b^2, \qquad (9)$$

where $k_{F_{\rm n}}$ and $k_{F_{\rm p}}$ are the Fermi momenta for neutrons and protons, respectively. Furthermore, the baryon density ρ_B is given by $\rho_B = 2k_F^3/(3\pi^2)$ using the Thomas-Fermi approximation. The static Klein-Gordon equations for nuclear matter become

$$m_\sigma^2 \sigma = -g_\sigma \rho_s - g_1 \sigma^2 - g_2 \sigma^3,$$

$$m_\omega^2 \omega = g_\omega \rho_B,$$

$$m_\rho^2 b = g_\rho \rho_3, \qquad (10)$$

where the scalar density ρ_s for the nuclear matter is given by

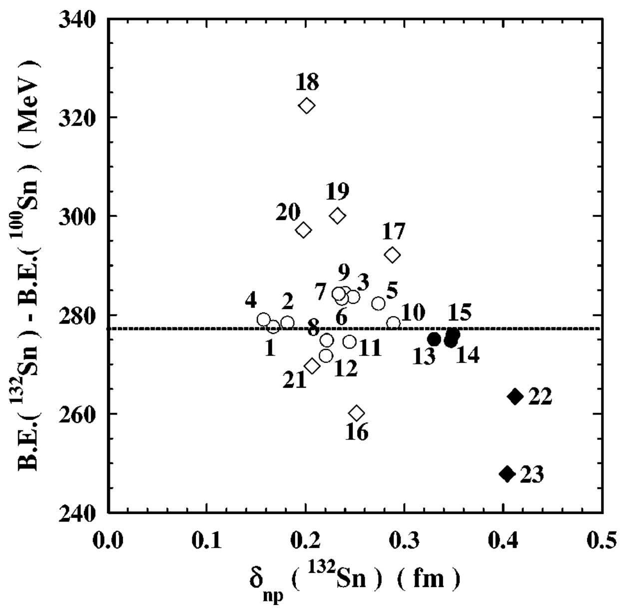

FIG. 1. The neutron skin thickness of ^{132}Sn and the binding energy difference between ^{132}Sn and ^{100}Sn are plotted for 18 parameter sets of the SHF model (open circles and open diamonds) and 5 parameter sets of the RMF model (filled circles and filled diamonds). The experimental binding energy difference is shown as a dotted line. The numbers are a shorthand notation for the different interactions: 1 for SI, 2 for SIII, 3 for SIV, 4 for SVI, 5 for Skya, 6 for SkM, 7 for SkM*, 8 for SLy4, 9 for MSkA, 10 for SkI3, 11 for SkI4, 12 for SkX, 13 for NLSH, 14 for NL3, 15 for NLC, 16 for SII, 17 for SV, 18 for Skyb, 19 for SGI, 20 for SGII, 21 for SLy10, 22 for NL1, and 23 for NL2.

$$\rho_s = \frac{2}{(2\pi)^3}\left[\int_0^{k_{F_{\rm n}}} + \int_0^{k_{F_{\rm p}}}\right]\frac{M^*}{(k^2 + M^{*2})^{1/2}} d^3k. \qquad (11)$$

Therefore the static Hamiltonian density in the nuclear matter becomes

$$\mathcal{H}_{\rm nm} = \frac{2}{(2\pi)^3}\left[\int_0^{k_{F_{\rm p}}} + \int_0^{k_{F_{\rm n}}}\right](k^2 + M^{*2})^{1/2}\, d^3k + \frac{g_\omega^2 \rho_B^2}{2m_\omega^2} + U(\sigma) + \frac{1}{2}m_\sigma^2\sigma^2 + \frac{g_\rho^2\rho_3^2}{2m_\rho^2}. \qquad (12)$$

In SHF calculations, the Hamiltonian density is derived analytically, while it is calculated numerically in RMF calculations.

The neutron skin thickness $\delta_{\rm np}$ and the binding energies obtained in the SHF and RMF models are plotted in Figs. 1 and 2 for ^{132}Sn and ^{208}Pb, respectively. Spherical symmetry is assumed for finite nuclei. The neutron skin thickness is defined as the difference between the root-mean-square neutron and proton radii,

$$\delta_{\rm np} = \sqrt{\langle r^2\rangle_{\rm n}} - \sqrt{\langle r^2\rangle_{\rm p}}. \qquad (13)$$

In Fig. 1, the horizontal axis is the neutron skin thickness $\delta_{\rm np}$ of ^{132}Sn and the vertical axis is the binding energy difference between ^{132}Sn and ^{100}Sn. Both ^{132}Sn and ^{100}Sn are doubly closed-shell nuclei like ^{208}Pb. Open circles and

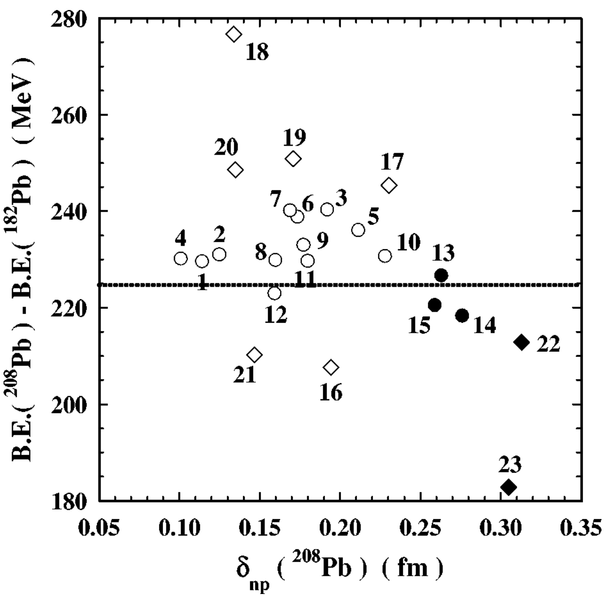

FIG. 2. The neutron skin thickness of ^{208}Pb and the difference between the binding energies of ^{208}Pb and ^{182}Pb are plotted for 18 parameter sets of the SHF model (open circles and open diamonds) and 5 parameter sets of the RMF model (filled circles and filled diamonds). The experimental binding energy difference is shown as a dotted line. See the caption of Fig. 1 for details.

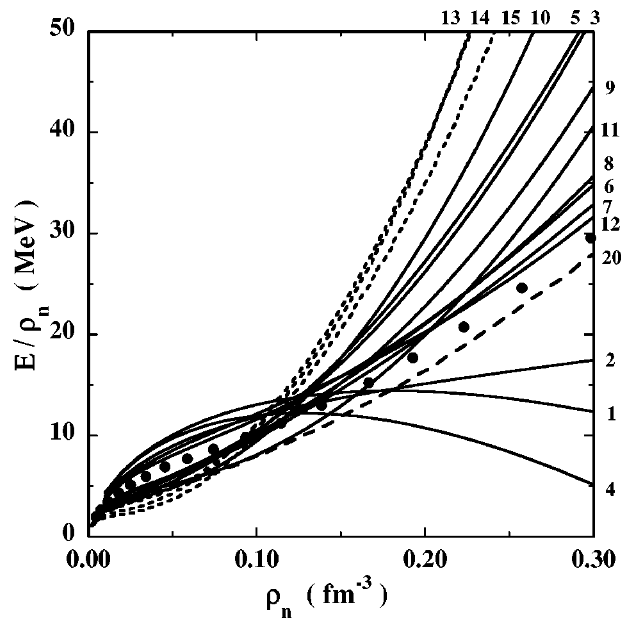

FIG. 3. The neutron equations of state are shown for the 12 parameter sets of the SHF model (solid lines) and 3 parameter sets of the RMF model (dashed lines) which in Figs. 1 and 2 were shown to reproduce the differences of experimental binding energies reasonably well. Filled circles correspond to the variational calculations using the v_{14} nucleon-nucleon potential and a phenomenological three-nucleon interaction, while the long-dashed curve corresponds to the SGII interaction. See the caption of Fig. 1 for details.

open diamonds are results with SHF parameter sets, while filled circles and filled diamonds are results obtained with the various RMF parameter sets. Each parameter set is designated by a specific number. The experimental binding energy difference is shown as a dotted line. The neutron radii have not yet been measured for ^{132}Sn and ^{100}Sn. In Fig. 2, results for ^{208}Pb and ^{182}Pb are presented. The open and filled diamonds in Figs. 1 and 2, represent the eight parameter sets, which do not reproduce the experimental binding energy difference between ^{132}Sn and ^{100}Sn and that between ^{208}Pb and ^{182}Pb to a reasonably good accuracy. They are therefore omitted in the subsequent studies.

Figure 3 shows the neutron equations of state for our different parameter sets, while the pressure of neutron matter is plotted as a function of neutron density in Fig. 4. In Figs. 3 and 4 the solid and dotted lines show the results with SHF and RMF models, respectively. We present results obtained with 13 SHF parameter sets (SI, SIII, SIV, SVI, Skya, SkM, SkM*, SkI3, SkI4, MSkA, SLy4, SkX, SGII) and 3 RMF parameter sets (NL3, NLSH, NLC). All except the SGII interaction reproduce well the experimental binding energy differences between ^{132}Sn and ^{100}Sn and between ^{208}Pb and ^{182}Pb as shown in Figs. 1 and 2, respectively. We plot the results obtained with SGII (long-dashed curves) in Figs. 3 and 4, since the SGII interaction gives almost equivalent results to those of the variational calculations using the v_{14} nucleon-nucleon potential together with a phenomenological three-nucleon interaction [32], which is fitted to reproduce nucleon-nucleon scattering data and the properties of nuclear matter. In Figs. 3 and 4 one can see large variations among different parameter sets. A general feature is that the RMF curves exhibit a much larger curvature than do the SHF curves, some of which even have negative curvature. Figures 3 and 4 show that results obtained with the SGII and SkX parameter sets are almost equivalent to the results of the variational calculations.

Next, we study the relation between the neutron skin thickness of finite nuclei and the pressures of neutron matter at $\rho_n = 0.1$ fm^{-3} and 0.2 fm^{-3}. Results for the pressures at $\rho_n = 0.1$ fm^{-3} and $\rho_n = 0.2$ fm^{-3} are given in Figs. 5(a) and 6(a) and Figs. 5(b) and 6(b), respectively. We plot in Figs. 5(b) and 6(b) the results at $\rho_n = 0.2$ fm^{-3} where the different interactions result in a wider range of pressures. The properties of nuclear matter at high densities are important for a unified description of neutron stars, from the outer crust down to the dense core [33]. Clear linear correlations are found between the neutron skin thickness δ_{np} and the pressure P of ^{208}Pb and ^{132}Sn in Figs. 5 and 6, respectively, with the parameter sets of the SHF and RMF models used in Figs. 3 and 4. In general, the RMF pressures are larger than those of SHF models, and the RMF models give the larger neutron skin thickness. The results at $\rho_n = 0.1$ fm^{-3} are consistent with the studies of Refs. [8,9]. Thus, experimental δ_{np} values would provide important constraints on the parameters used in SHF and RMF models. We fit linear functions to the data presented in each figure by the method of least squares and obtain

$$\delta_{np} = 1.09 \times 10^{-1} P + 7.76 \times 10^{-2} \quad \text{for} \quad {}^{208}\text{Pb} \quad \text{with}$$

$$\rho_n = 0.1 \text{ fm}^{-3} \; (r = 0.988, S = 7.96 \times 10^{-3}), \qquad (14)$$

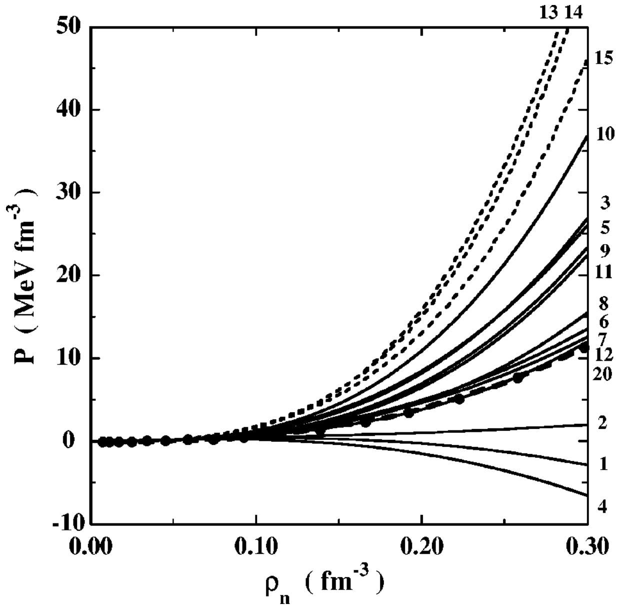

FIG. 4. The pressure of neutron matter as a function of neutron densities. The same parameter sets as those of Fig. 3 are used. The variational calculations with the v_{14} potential are shown by filled circles. The results of the SHF model are given by the solid lines, while those of the RMF model are given by the dashed lines. The long-dashed curve shows the results of the SGII interaction. See the caption of Fig. 1 for details.

$$\delta_{\rm np} = 1.02 \times 10^{-2} P + 1.15 \times 10^{-1} \quad \text{for} \quad {}^{208}\text{Pb} \quad \text{with} \quad \rho_{\rm n} = 0.2~\text{fm}^{-3}~(r = 0.986, S = 8.65 \times 10^{-3}), \tag{15}$$

$$\delta_{\rm np} = 1.21 \times 10^{-1} P + 1.29 \times 10^{-1} \quad \text{for} \quad {}^{132}\text{Sn} \quad \text{with} \quad \rho_{\rm n} = 0.1~\text{fm}^{-3}~(r = 0.987, S = 9.20 \times 10^{-3}), \tag{16}$$

$$\delta_{\rm np} = 1.13 \times 10^{-2} P + 1.71 \times 10^{-1} \quad \text{for} \quad {}^{132}\text{Sn} \quad \text{with} \quad \rho_{\rm n} = 0.2~\text{fm}^{-3}~(r = 0.977, S = 1.22 \times 10^{-2}), \tag{17}$$

where $\delta_{\rm np}$ and P are the neutron skin thicknesses in fm and the pressures in MeV fm^{-3}, respectively. The quantities r and S are the correlation coefficient and the standard deviation, respectively. These equations show that the coefficients of the P terms for ^{208}Pb are almost equal to those for ^{132}Sn for the two neutron matter densities $\rho_{\rm n}$=0.1 and 0.2 fm^{-3}.

We also study the relation between the pressure and the neutron skin thickness of several other nuclei, namely, ^{32}Mg, ^{38}Ar, ^{44}Ar, ^{100}Sn, ^{138}Ba, ^{182}Pb, and ^{214}Pb obtained in SHF + BCS calculations. In Fig. 7, ^{38}Ar (filled triangles), ^{138}Ba (crosses) and ^{208}Pb (filled circles) are stable nuclei, whereas ^{32}Mg (reversed open triangles), ^{44}Ar (open triangles), ^{132}Sn (open diamonds), and ^{214}Pb (open squares) are neutron-rich nuclei. The two nuclei ^{100}Sn (filled diamonds) and ^{182}Pb (open circles) are neutron deficient. This figure shows, in general, that the higher the third component of the nuclear isospin $T_z=(N-Z)/2$ is, the steeper the slope of the line is.

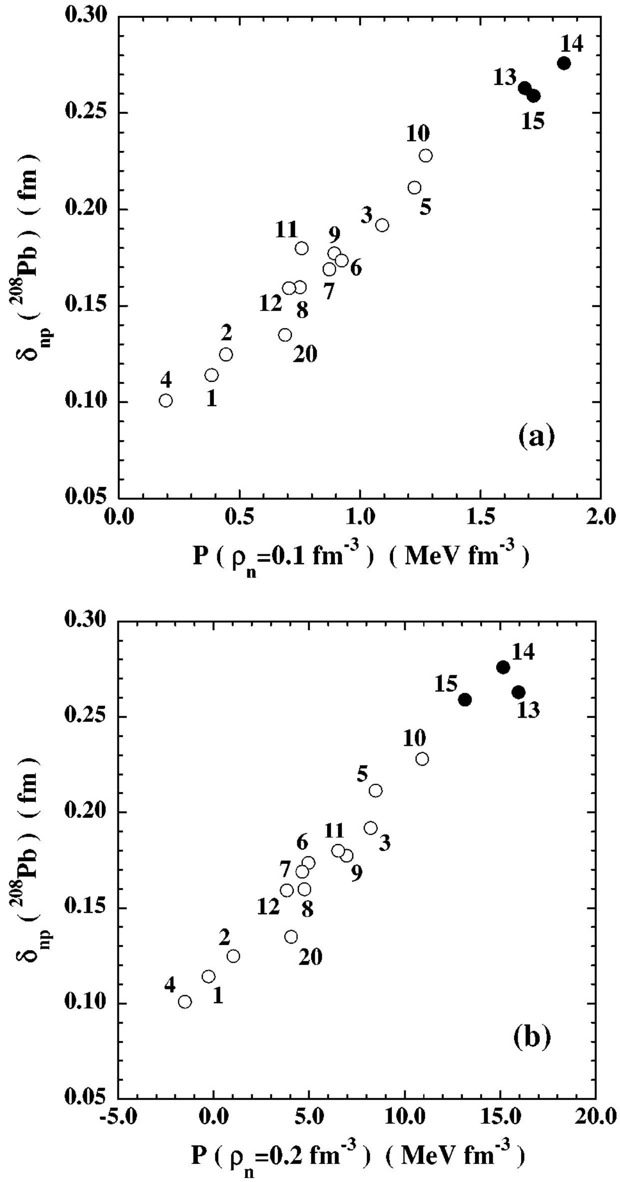

FIG. 5. The correlations between the pressures of neutron matter and the neutron skin thickness of ^{208}Pb obtained with the same SHF (open circles) and RMF (filled circles) parameter sets as were used in Fig. 3. (a) The result for pressure at $\rho_{\rm n}$=0.1 fm^{-3}, (b) that at $\rho_{\rm n}$=0.2 fm^{-3}. See the caption of Fig. 1 for details.

This isospin rule does not hold in ^{32}Mg. This is because the effect of the neutron-proton Fermi energy disparity dominates the increase in the neutron radii of neutron-rich light nuclei while the pressure plays a minor role, although the absolute magnitude of $\delta_{\rm np}$ is the largest in Fig. 7. It was pointed out in Ref. [34] that configuration mixing might play an important role in determining the neutron and proton radii in ^{32}Mg. However, the correlation between the neutron skin thickness and the pressure might not be changed by configuration mixing. The linear functions obtained from the fits to the data in Fig. 7 by the method of least squares behave in a similar way as those of ^{208}Pb and ^{132}Sn:

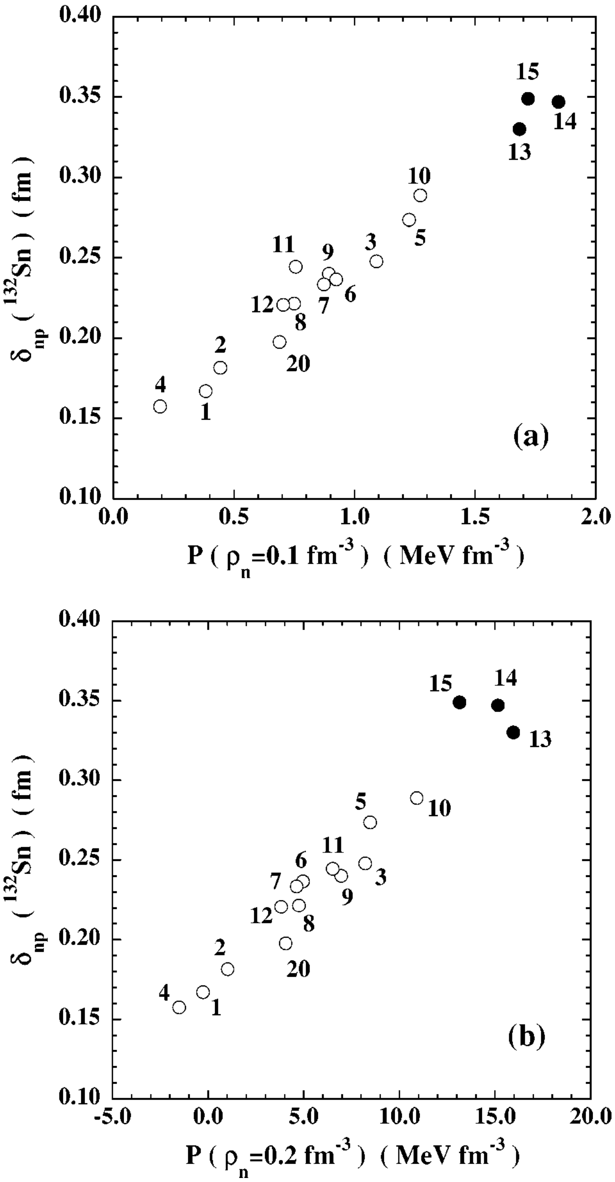

FIG. 6. The correlations between the pressures of neutron matter and the neutron skin thickness of ^{132}Sn obtained by use of the same SHF (open circles) and RMF (filled circles) parameter sets as were used in Fig. 3. (a) The result for pressure at ρ_n=0.1 fm^{-3}, (b) that at ρ_n=0.2 fm^{-3}. See the caption of Fig. 1 for details.

$$\delta_{np} = 4.85 \times 10^{-2}P + 2.44 \times 10^{-1} \quad \text{for}$$

$$^{32}\text{Mg } (r = 0.744, S = 1.33 \times 10^{-2}), \tag{18}$$

$$\delta_{np} = 3.64 \times 10^{-3}P + 1.19 \times 10^{-2} \quad \text{for}$$

$$^{38}\text{Ar } (r = 0.247, S = 4.34 \times 10^{-3}), \tag{19}$$

$$\delta_{np} = 6.82 \times 10^{-2}P + 1.28 \times 10^{-1} \quad \text{for}$$

$$^{44}\text{Ar } (r = 0.799, S = 1.56 \times 10^{-2}), \tag{20}$$

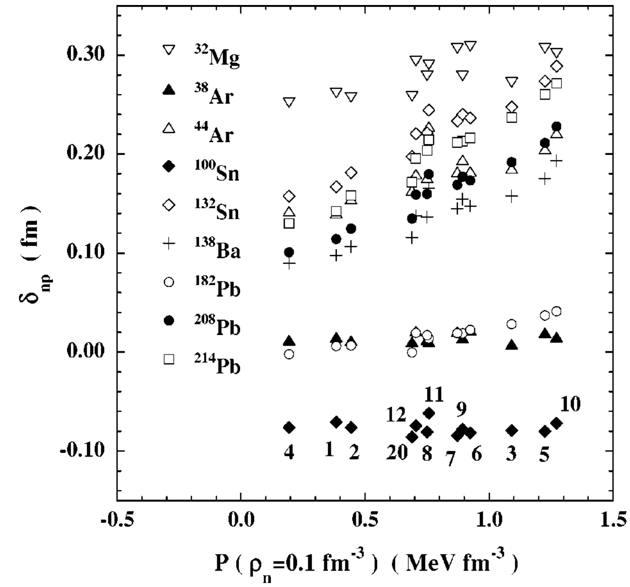

FIG. 7. The correlations between the pressures of neutron matter and the neutron skin thickness of ^{32}Mg (reversed open triangles), ^{38}Ar (filled triangles), ^{44}Ar (open triangles), ^{100}Sn (filled diamonds), ^{132}Sn (open diamonds), ^{138}Ba (crosses), ^{182}Pb (open circles), ^{208}Pb (filled circles), ^{214}Pb (open squares) for the pressure at ρ_n=0.1 fm^{-3}. The parameter sets of SHF model are the same as those of Fig. 3. See the caption of Fig. 1 for details.

$$\delta_{np} = -3.38 \times 10^{-3}P - 7.43 \times 10^{-3} \quad \text{for}$$

$$^{100}\text{Sn } (r = -0.168, S = 6.04 \times 10^{-3}), \tag{21}$$

$$\delta_{np} = 9.10 \times 10^{-2}P + 6.88 \times 10^{-2} \quad \text{for}$$

$$^{138}\text{Ba } (r = 0.938, S = 1.03 \times 10^{-2}), \tag{22}$$

$$\delta_{np} = 3.81 \times 10^{-2}\, P - 1.24 \times 10^{-2} \quad \text{for}$$

$$^{182}\text{Pb } (r = 0.922, S = 4.86 \times 10^{-3}), \tag{23}$$

$$\delta_{np} = 1.32 \times 10^{-1}P + 9.88 \times 10^{-2} \quad \text{for}$$

$$^{214}\text{Pb } (r = 0.981, S = 7.91 \times 10^{-3}). \tag{24}$$

Equations (19) and (21) show that the standard deviations S are larger than gradients of the linear correlations between the δ_{np} and the pressure P in ^{38}Ar and ^{100}Sn, so that the δ_{np} values look almost flat as a function of the pressure P. This is due to the fact that these two nuclei are close to the proton drip line and a high Coulomb barrier prevents an increase of δ_{np}. The correlations are weak in the neutron-rich T_Z=4 nuclei ^{32}Mg and ^{44}Ar in which the large difference between the proton and neutron Fermi energies is the main reason a sizable neutron skin is obtained.

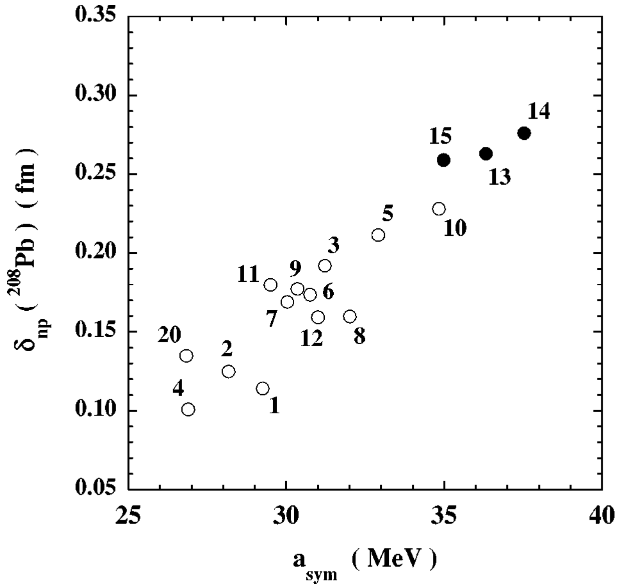

FIG. 8. The neutron skin thickness of ^{208}Pb vs the volume symmetry energy coefficient obtained with the same SHF (open circles) and RMF (filled circles) parameter sets as were used in Fig. 3. See the caption of Fig. 1 for details.

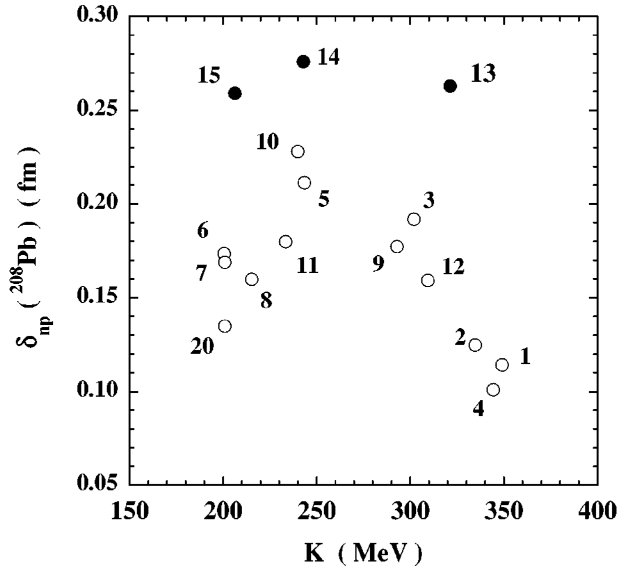

FIG. 9. The neutron skin thickness of ^{208}Pb vs the incompressibility of asymmetric nuclear matter. The SHF (open circles) and RMF (filled circles) parameter sets are the same as in Fig. 3. See the caption of Fig. 1 for details.

IV. NEUTRON SKIN THICKNESS AND SYMMETRY ENERGY COEFFICIENT

In this section, we study the correlation between the neutron skin thickness and the volume and surface symmetry energy coefficients in SHF and RMF models. Figure 8 shows a correlation between the neutron skin thickness of ^{208}Pb and the volume symmetry energy coefficient a_{sym}. In Fig. 8, we can see that there is an approximately linear correlation between δ_{np} and a_{sym}, although the mean square deviation is larger than that of Fig. 5; the correlation is somewhat weaker than those between the δ_{np} and the P values. The correlation between δ_{np} and a_{sym} was also discussed in Ref. [35] based on the mass formula. In neutron-rich nuclei, the wave functions of the excess neutrons have small components in nuclear center. Instead, large components of their wave functions are located in the outer surface region. This is caused essentially by the disparity of neutron-proton mean field potentials due to the asymmetry energy. Therefore, we can understand that the neutron skins of RMF having larger asymmetry energies are larger than those of SHF. It is also interesting to observe that one of the nuclear matter properties, namely, a_{sym}, has a close connection with the first derivative of EOS in neutron matter.

The incompressibility makes a crucial contribution to the nuclear matter EOS. We have investigated whether there is any correlation between the neutron skin thickness and the incompressibility K of asymmetric nuclear matter in Fig. 9. We found that there is essentially no correlation between the two quantities, as is seen in Fig. 9 where the ratio of neutron density to proton density for asymmetric nuclear matter is taken to be the same as the ratio of proton to neutron numbers of ^{208}Pb.

Finally, we study in Fig. 10 the relation between the δ_{np} and the surface symmetry energy coefficient $\varepsilon_{\mathrm{ss}}$ for the various SHF and RMF forces. The surface symmetry energy describes the surface properties of semi-infinite asymmetric nuclear matter. We find that for the SHF model a linear correlation between δ_{np} and $\varepsilon_{\mathrm{ss}}$ holds approximately although the mean square deviation is larger than the case of the volume symmetry energy. Detailed formulas of the surface symmetry energies are given in the Appendix.

V. SUMMARY

We studied relations between the neutron skin thickness and the pressure of the EOS in neutron matter obtained in

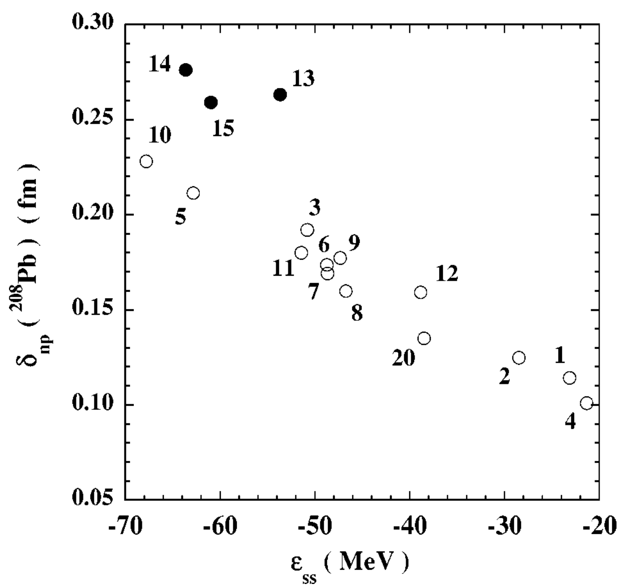

FIG. 10. The neutron skin thickness of ^{208}Pb vs the surface symmetry energy coefficient of semi-infinite asymmetric nuclear matter. The SHF (open circles) and RMF (filled circles) parameter sets are the same as in Fig. 3. See the caption of Fig. 1 for details.

SHF and RMF models. A strong linear correlation between the neutron skin thickness and the pressure of neutron matter as given by the EOS is obtained for stable nuclei such as ^{132}Sn and ^{208}Pb. On the other hand, the correlations between the two quantities in unstable nuclei such as ^{32}Mg and ^{44}Ar are found to be weaker. We pointed out that, in general, the pressure derived from the RMF model is much higher than that obtained from the SHF model. Also the neutron skin thickness of both stable and unstable nuclei is much larger in the RMF models than in the SHF models for stable nuclei. Thus, experimental data on the neutron skin thickness give critical information both on the EOS pressure in neutron matter and on the relative merits of the various parameter sets used in mean-field models. We also studied relations between the neutron skin thickness and other nuclear matter properties such as the nuclear incompressibility and the symmetry energy coefficients of SHF and RMF models. We found clearly a correlation between the neutron skin thickness and the symmetry energy coefficients, while there is essentially no correlation between the nuclear incompressibility K and the neutron skin thickness $\delta_{\rm np}$. Further studies of the relation between the pressure of neutron matter and the symmetry energy coefficients are in progress.

ACKNOWLEDGMENTS

We thank Peter Möller for careful reading of the manuscript. We thank also I. Hamamoto, W. Nazarewicz, and K. Matsuyanagi for useful discussions. This work was supported in part by the Japanese Ministry of Education, Science, Sports and Culture by Grant-in-Aid for Scientific Research under the program number (C(2)) 12640284.

APPENDIX: VOLUME AND SURFACE SYMMETRY ENERGY OF SHF AND RMF

The symmetry energy coefficient $a_{\rm sym}$ is defined as the second derivative of the Hamiltonian density $\mathcal{H}$,

$$a_{\rm sym} = \frac{1}{2}\lim_{I\to 0}\frac{\partial^2}{\partial I^2}\left(\frac{\mathcal{H}}{\rho}\right) \tag{A1}$$

with respect to the asymmetry parameter $I=(N-Z)/A$. The kinetic energy part of $\mathcal{H}$ is evaluated for semi-infinite nuclear matter by the extended Thomas-Fermi approximation,

$$\tau_q = \alpha\rho_q^{5/3} + \beta\frac{(\nabla\rho_q)^2}{\rho_q} + \gamma\Delta\rho_q (q=n,p) \tag{A2}$$

with $\alpha=\frac{3}{5}(3\pi^2)^{2/3}$, $\beta=\frac{1}{18}$, $\gamma=\frac{1}{3}$ [6]. In SHF models, the symmetry energy coefficient is given by

$$a_{\rm sym} = \frac{\hbar^2}{6m}\left(\frac{3\pi^2}{2}\right)\rho^{2/3} - \frac{1}{8}t_0(1+2x_0)\rho - \frac{1}{48}t_3(1+2x_3)\rho^{\alpha+1} - \frac{1}{24}\left(\frac{3\pi^2}{2}\right)^{2/3}\{3t_1x_1 - t_2(4+5x_2)\}\rho^{5/3}, \tag{A3}$$

while in RMF models, it becomes

$$a_{\rm sym} = \frac{3\pi^2 A}{16 g_\sigma k_F^3}\left[3(m_\sigma^2\phi + g_1\phi^2 + g_2\phi^3) - \frac{M^*}{g_\sigma}(m_\sigma^2 + 2g_1\phi + 3g_2\phi^2)\right] + \frac{g_\rho^2 k_F^3}{3\pi^2 m_\rho^2} + \frac{1}{24}\left[-\frac{k_F^4}{B^3} + \frac{5k_F^2}{B} + \frac{9M^*A}{B}\right], \tag{A4}$$

where A and B are given by

$$A = \left[\frac{2g_\sigma k_F}{\pi^2}\left(B - \frac{M^{*2}}{B}\right) + \frac{3}{M^*}(m_\sigma^2\phi + g_1\phi^2 + g_2\phi^3) - \frac{1}{g_\sigma}(m_\sigma^2 + 2g_1\phi + 3g_2\phi^2)\right]^{-1}\left[-\frac{2k_F^5 M^*}{9B^3}\right], \tag{A5}$$

$$B = \sqrt{k_F^2 + M^{*2}}. \tag{A6}$$

It is known that the surface symmetry energy influences the surface properties of semi-infinite asymmetric nuclear matter. To second order in I the surface energy $\varepsilon_{\rm s}(I)$ is given by

$$\varepsilon_{\rm s}(I) = \varepsilon_{\rm s}(0) + \varepsilon_{\rm ss}I^2. \tag{A7}$$

The quantity $\varepsilon_{\rm ss}$ is given by

$$\varepsilon_{\rm ss} = 8\pi r_{\rm nm}^2\int_{-\infty}^{\infty}\rho[\varepsilon_\delta(\rho) - J]dx + 2\varepsilon_{\rm s}(0)\frac{L}{K}, \tag{A8}$$

where $\varepsilon_\delta(\rho)$ is the isovector part of Hamiltonian density $\mathcal{H}$ up to second order in $(\rho_{\rm n}-\rho_{\rm p})$, J is the nuclear matter symmetry energy, K is the nuclear incompressibility, and L is defined by

$$L = 3\rho_{\rm nm}\frac{d\varepsilon_\delta(\rho)}{d\rho_{\rm nm}}. \tag{A9}$$

The isovector density ε_δ can be expressed as a Taylor expansion around $\rho_{\rm nm}$:

$$\varepsilon_\delta(\rho) = J + \frac{L}{3}\frac{\rho-\rho_{\rm nm}}{\rho_{\rm nm}} + \frac{K_{\rm sym}}{18}\left(\frac{\rho-\rho_{\rm nm}}{\rho_{\rm nm}}\right)^2. \tag{A10}$$

The quantity $K_{\rm sym}$ is defined by

$$K_{\rm sym} = 9\rho_{\rm nm}^2\frac{d^2\varepsilon_\delta(\rho)}{d\rho_{\rm nm}^2}. \tag{A11}$$

The surface symmetry energy $\varepsilon_{\rm ss}$ is evaluated to be

$$\varepsilon_{\rm ss} = -\frac{2a}{r_{\rm nm}}\left(L - \frac{1}{12}K_{\rm sym}\right) + 2\varepsilon_{\rm s}(0)\frac{L}{K} \tag{A12}$$

by inserting Eq. (A10) [36] and the Fermi-type density distribution

$$\rho = \frac{\rho_{\rm nm}}{1+\exp(x/a)} \equiv \rho_{\rm nm}y \tag{A13}$$

into Eq. (A8). In order to determine the surface diffuseness a, the nuclear matter part of the Hamiltonian density is expressed in terms of the nuclear incompressibility K, which gives the relation

$$\mathcal{H} = \rho\left[\frac{K}{18}\left(1-\frac{\rho}{\rho_{\rm nm}}\right)^2 - E_0\right] + A(\rho)(\nabla\rho)^2, \quad \text{(A14)}$$

where E_0 is the binding energy. The derivative terms in Eq. (A14) are evaluated assuming the density is given by a Fermi distribution (A13) as

$$\mathcal{H} = \rho_{\rm nm}\, y\left[\frac{K}{18}(1-y)^2 - E_0\right] + A'(y)\left(\frac{dy}{dx}\right)^2. \quad \text{(A15)}$$

The parameter a of Fermi distribution y can be obtained by solving the differential equation

$$y(1-y) = \left[\frac{18}{K}\left(\frac{\hbar^2\beta}{2m} + \frac{1}{2}B\rho_{\rm nm}\, y + C\rho_{\rm nm}^2\sum_{i=1}^{2}\frac{u_i y^2}{1+v_i\rho_{\rm nm} y}\right)\right]^{1/2}\left(\frac{dy}{dx}\right), \quad \text{(A16)}$$

which is derived by taking the functional derivative of Eq. (A15) with respect to y, where

$$B = \frac{1}{4}\{t_1(1-x_1)+3t_2(1+x_2)\}(\beta-\gamma)\frac{1+I^2}{2} + \frac{1}{2}\left\{t_1\left(1+\frac{1}{2}x_1\right) + t_2\left(1+\frac{1}{2}\right)\right\}(\beta-\gamma)\frac{1-I^2}{2} + \frac{3}{16}\{t_1(1-x_1)-t_2(1+x_2)\} \times\frac{1+I^2}{2} + \frac{1}{8}\left\{3t_1\left(1+\frac{1}{2}x_1\right) - t_2\left(1+\frac{1}{2}x_2\right)\right\}\frac{1-I^2}{2},$$

$$C = -\frac{mW_0^2}{32\hbar^2},$$

$$u_{1(2)} = 9 \pm 11I + 7I^2 \pm 5I^3,$$

$$v_{1(2)} = \frac{m}{8\hbar^2}[3(t_1+t_2) \mp \{t_1(1+2x_1) - t_2(1+2x_2)\}].$$

Equation (A16) is solved with the boundary condition

$$\lim_{y\to 1}\frac{dy}{dx} = 0. \quad \text{(A17)}$$

The surface diffuseness is given by the integral

$$a = \int_{-\infty}^{\infty} y(1-y)dx. \quad \text{(A18)}$$

In the RMF model, the Hamiltonian density is given by

$$\mathcal{H} = \frac{2}{(2\pi)^3}\left[\int_0^{k_{Fn}} + \int_0^{k_{Fp}}\right](k^2+M^{*2})^{1/2}d^3k + g_\omega\omega\rho_B + g_\rho b\rho_3 + \frac{1}{2}m_s^2\sigma^2 + \frac{1}{2}(\nabla\sigma)^2 + U(\sigma) - \frac{1}{2}(\nabla\omega)^2 - \frac{1}{2}m_\omega^2\omega^2 - \frac{1}{2}(\nabla b)^2 - \frac{1}{2}m_\rho^2 b^2. \quad \text{(A19)}$$

We approximate the Hamiltonian density for nuclear matter $\mathcal{H}_{\rm nm}$ given in Eq. (12) by

$$\rho_B\left[\frac{K}{18}\left(1-\frac{\rho_B}{\rho_{\rm nm}}\right)^2 - E_0\right]. \quad \text{(A20)}$$

Therefore, in this approximation the Hamiltonian density is given by

$$\begin{aligned}\mathcal{H} &= \frac{2}{(2\pi)^3}\left[\int^{k_{F_n}} + \int^{k_{F_p}}\right](k^2+M^{*2})^{1/2}d^3k + g_\omega\omega\rho_B + g_\rho b_{\rho_3} + \frac{1}{2}m_s^2\sigma^2 + \frac{1}{2}(\nabla\sigma)^2 + U(\sigma) - \frac{1}{2}(\nabla\omega)^2 - \frac{1}{2}m_\omega^2\omega^2 \\ &\quad - \frac{1}{2}(\nabla b)^2 - \frac{1}{2}m_\rho^2 b^2 - \mathcal{H}_{\rm nm} + \rho_B\left[\frac{K}{18}\left(1-\frac{\rho_B}{\rho_{\rm nm}}\right)^2 - E_0\right] \\ &= \rho_B\left[\frac{K}{18}\left(1-\frac{\rho_B}{\rho_{\rm nm}}\right)^2 - E_0\right] - \frac{g_\omega^2\rho_B^2}{2m_\omega^2} - \frac{g_\rho^2\rho_3^2}{2m_\rho^2} + g_\omega\omega\rho_B + g_\rho b\rho_3 + \frac{1}{2}(\nabla\sigma)^2 - \frac{1}{2}(\nabla\omega)^2 - \frac{1}{2}m_\omega^2\omega^2 - \frac{1}{2}(\nabla b)^2 \\ &\quad - \frac{1}{2}m_\rho^2 b^2. \end{aligned} \quad \text{(A21)}$$

We assume a Fermi-type density distribution for the baryon density ρ_B such as in the SHF calculations,

$$\rho_B = \frac{\rho_{\rm nm}}{1+\exp(x/a)} \equiv \rho_{\rm nm}\, y. \quad \text{(A22)}$$

The Fermi distribution y is the solution to the differential equation

$$y(1-y)^2 = \frac{9}{K\rho_{\rm nm}}\left[\frac{g_\omega^2\rho_{\rm nm}^2 y^2}{m_\omega^2} + \frac{g_\rho^2\rho_{\rm nm}y^2I^2}{m_\rho^2} - 3g_\omega\rho_{\rm nm}y\omega - 3g_\rho\rho_{\rm nm}Iyb + 2m_\omega^2\omega^2 + 2m_\rho^2b^2 - \sigma(m_\sigma^2\sigma + g_\sigma\rho_{\rm s} + g_2\sigma^2 + g_3\sigma^3)\right], \quad \text{(A23)}$$

where σ, ω, and ρ meson fields are given by solving the Klein-Gordon equations. Finally, we obtain the surface diffuseness from the integral

$$\frac{a}{2} = \int_{-\infty}^{\infty} y(1-y)^2dx. \quad \text{(A24)}$$

[1] G. Fricke *et al.*, At. Data Nucl. Data Tables **60**, 177 (1995).
[2] L. Ray, G. W. Hoffmann, and W. R. Coker, Phys. Rep. **212**, 223 (1992).
[3] T. Suzuki *et al.*, Phys. Rev. Lett. **75**, 3241 (1995).
[4] C. J. Horowitz, S. J. Pollock, P. A. Souder, and R. Michaels, Phys. Rev. C **63**, 025501 (2001).
[5] W. D. Myers and W. J. Swiatecki, Nucl. Phys. **A336**, 267 (1980); M. Farine, J. Cofe, and J. M. Pearson, Phys. Rev. C **24**, 303 (1981); S. Stringari and E. Lipparini, Phys. Lett. **117B**, 141 (1982).
[6] J. Treiner and H. Krivine, Ann. Phys. (N.Y.) **170**, 406 (1986).
[7] C. J. Horowitz and J. Piekarewicz, Phys. Rev. Lett. **86**, 5647 (2001).
[8] A. Brown, Phys. Rev. Lett. **85**, 5296 (2000); (private communication).
[9] S. Typel and B. A. Brown, Phys. Rev. C **64**, 027302 (2001).
[10] R. J. Furnstahl, Nucl. Phys. **A706**, 85 (2002).
[11] T. H.R. Skyrme, Nucl. Phys. **9**, 615 (1959).
[12] D. Vautherin and D. M. Brink, Phys. Rev. C **5**, 626 (1972).
[13] M. Beiner, M. Flocard, Nguyen Van Giai, and P. Quentin, Nucl. Phys. **A238**, 28 (1975).
[14] H. S. Köhler, Nucl. Phys. **A258**, 301 (1976).
[15] H. Krivine, J. Treiner, and O. Bohigas Nucl. Phys. **A336**, 155 (1980).
[16] Nguyen Van Giai and H. Sagawa, Phys. Lett. **106B**, 379 (1981).
[17] J. Bartel, P. Quentin, M. Brack, C. Guet, and H.-B. Hakansson, Nucl. Phys. **A386**, 79 (1982).
[18] P.-G. Reinhard and H. Flocard, Nucl. Phys. **A584**, 467 (1994).
[19] M. M. Sharma, G. Lalazissis, J. König, and P. Ring, Phys. Rev. Lett. **74**, 3744 (1995).
[20] E. Chabanat, P. Bonche, P. Haensel, J. Meyer, and R. Schaeffer, Nucl. Phys. **A635**, 231 (1998).
[21] P. Bonche, H. Flocard, P. H. Heenen, S. J. Krieger, and M. S. Weiss, Nucl. Phys. **A443**, 39 (1985).
[22] P. G. Reinhard, M. Rufa, J. Maruhn, W. Greiner, and J. Friedrich, Z. Phys. A **323**, 13 (1986).
[23] J. D. Walecka, Ann. Phys. (N.Y.) **83**, 469 (1974).
[24] C. J. Horowitz and B. D. Serot, Nucl. Phys. **A368**, 503 (1981).
[25] B. D. Serot and J. D. Walecka, Adv. Nucl. Phys. **16**, 1 (1986).
[26] Y. K. Gambhir, P. Ring, and A. Thimet, Ann. Phys. (N.Y.) **198**, 132 (1990).
[27] B. D. Serot, Rep. Prog. Phys. **55**, 1855 (1992); P. G. Reinhard, *ibid.* **52**, 439 (1992).
[28] J. Boguta and A. R. Bodmer, Nucl. Phys. **A292**, 413 (1977).
[29] G. A. Lalazissis, J. König, and P. Ring, Phys. Rev. C **55**, 540 (1997).
[30] M. M. Sharma, M. A. Nagarajan, and P. Ring, Phys. Lett. B **312**, 377 (1993).
[31] B. D. Serot and J. D. Walecka, Int. J. Mod. Phys. E **6**, 515 (1997).
[32] B. Friedman and V. R. Pandharipande, Nucl. Phys. **A361**, 502 (1981).
[33] G. Baym, H. A. Bethe, and C. J. Pethick, Nucl. Phys. **A175**, 225 (1971).
[34] R. R. Rodriguez-Guzman, J. L. Egido, and L. M. Robledo, Phys. Rev. C **62**, 054319 (2000).
[35] P. Danielewicz, Nucl. Phys. **A727**, 233 (2003).
[36] H. Krivine and J. Treiner, Phys. Lett. **124B**, 127 (1983).